

Control Strategy to Maximize the Power Capability of PV Three-Phase Inverters During Voltage Sags

Jorge Luis Sosa, Miguel Castilla, Jaume Miret, *Member, IEEE*, José Matas, and Y. A. Al-Turki

Abstract—Under voltage sags, grid-tied photovoltaic inverters should remain connected to the grid according to low-voltage ride-through requirements. During such perturbations, it is interesting to exploit completely the distributed power provisions to contribute to the stability and reliability of the grid. In this sense, this paper proposes a low-voltage ride-through control strategy that maximizes the inverter power capability by injecting the maximum-rated current during the sag. To achieve this objective, two possible active power situations have been considered, i.e., high- and low-power production scenarios. In the first case, if the source is unable to deliver the whole generated power to the grid, the controller applies active power curtailment to guarantee that the maximum rated current is not surpassed. In the second case, the maximum allowed current is not reached, thus, the control strategy determined the amount of reactive power that can be injected up to reach it. The control objective can be fulfilled by means of a flexible current injection strategy that combines a proper balance between positive- and negative-current sequences, which limits the inverter output current to the maximum rated value and avoid active power oscillations. Selected experimental and simulation results are reported in order to validate the effectiveness of the proposed control strategy.

Index Terms—Distributed PV generation, low-voltage ride-through, maximum-rated current, reactive power injection, voltage sag.

I. INTRODUCTION

IN recent years, environmental issues are increasing significantly the number of grid-connected distributed generation (DG) systems [1], [2]. However, the large-scale integration of DG systems can introduce a negative impact on the overall stability and reliability of the grid infrastructure, especially under grid fault conditions. In this sense, grid codes (GCs) of countries with high penetration level of DG have defined the profile of the faults that these systems should withstand, and the procedure that they should follow under such situations.

Manuscript received February 16, 2015; revised May 19, 2015; accepted June 22, 2015. Date of publication July 1, 2015; date of current version November 30, 2015. This work was supported in part by the Ministerio de Economía y Competitividad of Spain and FEDER funds under Grant ENE2012-37667-C02-02, the Programa Iberoamericano de Ciencia y Tecnología para el Desarrollo under Grant 713RT0475, and the Deanship of Scientific Research, King Abdulaziz University, Jeddah, under Grant 24-135-35-HiCi. Recommended for publication by Associate Editor L. Chang

J. L. Sosa is with the Scientific Instrumentation Laboratory, Universidad de los Andes, Mérida 5101, Venezuela (e-mail: jorgesosa5@gmail.com).

M. Castilla and J. Miret are with the Department of Electronic Engineering, Technical University of Catalonia, Vilanova i la Geltrú 08800, Spain (e-mail: miguel.castilla@upc.edu; jaume.miret@upc.edu).

J. Matas is with the Department of Electronic Engineering, Technical University of Catalonia, Vilanova i la Geltrú 08800, Spain; He is also working with the Renewable Energy Research Group, King Abdulaziz University, Jeddah, Saudi Arabia (e-mail: jose.matas@upc.edu).

Y. A. Al-Turki is with the Renewable Energy Research Group, King Abdulaziz University, Jeddah 22254, Saudi Arabia (e-mail: yaturki@yahoo.com).

Color versions of one or more of the figures in this paper are available online at <http://ieeexplore.ieee.org>.

Digital Object Identifier 10.1109/TPEL.2015.2451674

In compliance with these requirements, DG sources must remain connected to the grid during voltage sags, following a predefined time/sag-depth profile before disconnection, which is known as low-voltage ride-through (LVRT). Additionally, wind GCs require the injection of the reactive power to support the grid voltage and to reduce the possibility of voltage collapse [3]–[5]. Consequently, it is expected that the continuously increasing number of grid-connected DG will promote new requirements in GCs. Upcoming GCs could demand also reactive power injection from distributed PV systems to fully exploit the reactive power provisions [4]–[6].

Under these requirements, different LVRT strategies have been proposed to enhance the performance of DG during voltage sags [7]–[17]. Most of reported works are based on symmetric sequences, since their use increases the flexibility and leads to achieve particular control objectives such as the mitigation of active and reactive power oscillations, voltage support, and peak current limitation.

As presented in [7] and [8], by means of specific strategies it is possible to obtain different power quality levels at the point of common coupling (PCC) in terms of instantaneous active and reactive power oscillations. However, avoiding active power oscillations results more favorable to the DG performance, since the active power oscillations are reflected as ripple in the dc-link voltage and could cause sudden disconnection of the voltage source inverter (VSI) if the maximum/minimum dc-link voltage is surpassed/under passed.

In voltage support strategies, the priority is to deliver only the reactive power during the sag. It can be attributed to the major impact that the reactive current can cause on the PCC voltages when a weak grid is considered. Depending on the type of sag, different reactive power strategies can be applied [9]–[11]. In [9], a reference-current generation algorithm that provides flexible voltage support was introduced. An improvement of [9] although limited to symmetric sags was presented in [10], where the PCC voltages can be restored if the DG system supplies enough reactive current. The authors in [11] present a voltage control scheme that can be used under any type of sag.

To avoid disconnection of the DG source due to overcurrent, the injected phase currents must be safely controlled at any time. In this regard, different strategies have been proposed. The control method presented in [12] ensures minimum peak values in the grid-injected currents when the whole generated power is delivered to the grid. However, current harmonic distortion was increased to meet the control objectives and the resulting minimum values always exceeded the VSI-rated current. In [13] and [14], the injection strategies avoid over current tripping, but the maximum output current was only related to the maximum reactive power delivered by the VSI under unbalanced grid conditions. As a drawback, the source is unable to deliver the active power production. Moreover, the active and reactive power present

oscillations at twice the grid frequency. The approach presented in [15] is based on the virtual flux estimation method. In this paper, different active and reactive power injection strategies have been proposed, however, not all of them ensure maximum current limitation. In [16] and [17], more flexible controllers have been proposed. These controllers provide different LVRT services by injecting active and reactive power by means of positive and negative sequences while maintaining the injected current safely controlled to a predefined maximum value. However, the control algorithms are complex when comparing with previous schemes.

This paper proposes a compact LVRT control strategy that guarantees the complete use of the power capabilities of the distributed PV system under voltage sags. The proposal comprises a set of reference currents that provides flexible positive and negative active and reactive power injection characteristics that can be tuned to fulfill two objectives during voltage sags: first, to inject maximum rated current independently of the sag profile and, second, to avoid active power oscillations. Both objectives will be always accomplished, although the achievement of first objective could be affected by the amount of the generated power. In this concern, two main possible scenarios may be considered, i.e., high- and low-power production scenarios. In the first case, the injection of the maximum current can be achieved delivering only active power, which is in compliance with present PV GCs. Moreover, if the source is unable to deliver the whole generated power, the control strategy applies active power curtailment to avoid surpass the maximum rated current and avoid disconnection due to overcurrent. In the second case, a combination of active and reactive power will be injected to reach the inverter maximum rated current. Therefore, the PV system can provide support to the grid during the fault. Although actual PV GCs do not require reactive power injection, this functionality could contribute to a better integration of distributed resources in the near future.

Some of the reviewed control strategies provide peak-current limitation and flexible operation under voltage sags. However, none of the presented strategies so far is able to determine the reference currents that optimize the VSI power capabilities in an easy manner with simple and compact reference expressions as presented here. Therefore, control simplicity is one of the remarkable contributions of this paper.

This paper is organized as follows. Section II describes the grid-connected DG system, analyzes the PCC voltages and inverter currents under a voltage sag event, and describes the GC requirements that must be applied under this situation. Section III exposes the conditions that give rise to control objectives and proposes a strategy to achieve it. Section IV develops the theoretical basis of the control proposal. Section V corroborates the expected features of the proposed controller by means of selected simulation and experimental results. Also, a discussion of the outstanding characteristics of the proposed strategy is presented, including a comparison with reported peak current limitation controllers. Section VI presents the conclusions of this paper.

II. GRID-CONNECTED INVERTERS UNDER VOLTAGE SAGS

This section deals with the description and characterization of the grid-connected VSI under voltage sags. Also, the basic GC requirements during these disturbances are described.

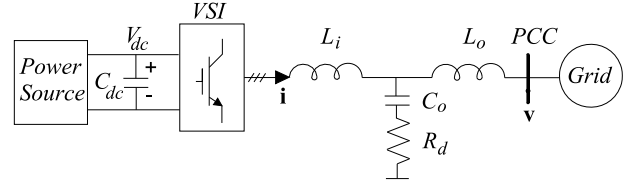


Fig. 1. Diagram of a grid-connected DG.

A. Grid-Connected Three-Phase Inverter

A typical configuration of grid-connected DG based on renewable resources is shown in Fig. 1 [2]. Basically, it is composed by a source, a large dc-link capacitor employed for decoupling the source and the converter, and a three-phase three-wire VSI connected to the PCC. The inverter uses an *LCL* filter to reduce the high-frequency commutation harmonics [18], [19]. Commonly, the *LCL* filter includes a set of damping resistors in series with the capacitors in order to mitigate resonance effects [18]. The voltage in the dc link is regulated to extract the maximum power from the source using an outer dc-link voltage controller, which provides the generated active power reference P_G that should be injected into the grid. This controller has been widely studied in the literature, and thus, it is not described in this paper [19], [20].

B. Voltage Sag Characterization

A voltage sag is a short-time reduction of the rms voltage magnitudes in one or more grid phases which can be caused by different types of line faults (phase to ground short-circuit, phase to phase to ground short circuit), overload, or power-up of large motors [21]–[23]. During voltage sags, the VSI suffers from a severe perturbation that can compromise its functionality and reliability. For this reason, the voltage and current vectors at the PCC must be properly characterized in order to deal with such event.

The instantaneous PCC phase voltages during voltage sags can be described as the addition of positive-, negative-, and zero-symmetric sequences. By means of Clarke transformation, the instantaneous PCC phase voltages can be expressed in the stationary reference frame (SRF) as

$$v_\alpha = v_\alpha^+ + v_\alpha^- = V^+ \cos(\omega t + \delta^+) + V^- \cos(\omega t + \delta^-) \quad (1)$$

$$v_\beta = v_\beta^+ + v_\beta^- = V^+ \sin(\omega t + \delta^+) - V^- \sin(\omega t + \delta^-) \quad (2)$$

where v_α and v_β are the SRF components of the measured voltage at PCC, v_α^+ , v_β^+ , and v_α^- , v_β^- are the SRF positive- and negative-voltage sequences, respectively, V^+ and V^- are the sequences amplitudes, ω is the grid angular frequency, and δ^+ and δ^- are the initial phase angles of positive- and negative-sequences, respectively. Note that the zero sequence is not considered here, since it is not present in three-wire systems [8].

There are different types of voltage sags, which can be characterized by the sequences amplitudes, V^+ , V^- , and by the sequence phase angle δ . The magnitudes of these parameters can be determined using the SRF theory [22], [23], as

$$V^+ = \sqrt{(v_\alpha^+)^2 + (v_\beta^+)^2} \quad (3)$$

$$V^- = \sqrt{(v_\alpha^-)^2 + (v_\beta^-)^2} \quad (4)$$

$$\delta = \delta^+ - \delta^- = \cos^{-1} \left(\frac{v_\alpha^+ v_\alpha^- - v_\beta^+ v_\beta^-}{V^+ V^-} \right). \quad (5)$$

C. Requirements for DG systems Under Voltage Sags

Under normal grid conditions, VSI delivers all the generated active power into the grid by controlling the amount of the injected current. During voltage sags, complementary services can be required by the GCs to increase the grid quality and reliability. Wind GCs require LVRT capabilities and support the grid with some amount of reactive current injection. This amount varies depending on the regulations of each country; in extreme cases, it can arrive to 100%. Furthermore, depending on the sag profile, GCs also require active and reactive power injection to simultaneously feed and support the grid [3]–[5]. Present GCs for PV systems only require the injection of the active power. However, reactive power injection could be demanded in the near future to fully exploit the reactive power provisions of distributed PV systems [4], [6].

III. PROBLEM FORMULATION

The purpose of this section is to explain the conditions that have set the foundation of the proposed current injection strategy and the objectives that can be reached. Furthermore, the control algorithm that leads to its practical implementation is presented.

A. Power Injection During Voltage Sags

According to the power theory [24], [25], the instantaneous active and reactive powers injected to the grid by a three-phase VSI depends on the injected currents and the voltage vectors (\mathbf{i} , \mathbf{v}) at the PCC. Thus, the instantaneous power can be defined as

$$p = \frac{3}{2}(v_\alpha i_\alpha + v_\beta i_\beta) \quad (6)$$

$$q = \frac{3}{2}(v_\beta i_\alpha - v_\alpha i_\beta). \quad (7)$$

Additionally, the VSI current references can be decomposed in active and reactive components as

$$i_\alpha^* = i_\alpha^*(p) + i_\alpha^*(q) \quad (8)$$

$$i_\beta^* = i_\beta^*(p) + i_\beta^*(q). \quad (9)$$

In compliance with present GCs, the PV systems must only inject the active power into the grid. To achieve this requirement, the following set of reference currents in the SRF can be used [26]

$$i_\alpha^*(p) = \frac{2}{3} \frac{v_\alpha^+}{(V^+)^2} P^* \quad (10)$$

$$i_\beta^*(p) = \frac{2}{3} \frac{v_\beta^+}{(V^+)^2} P^*. \quad (11)$$

In this scheme, the reference currents follow the positive-sequence voltage. Thus, the resulting currents are balanced and free of harmonics. However, during unbalanced voltage sags, this strategy introduces an oscillation in the injected active

power at twice the grid frequency which affects negatively the dc-link voltage and may cause dc overvoltage problems [25].

During the sag, the amplitude of the positive sequence V^+ will be reduced. Consequently, according to (10) and (11), the injected currents will increase to maintain the same amount of injected power previous to the sag. However, this conventional response may lead to tripping or damage of the converter because the reference currents might surpass the inverter maximum rated current. In this situation, the source is unable to inject the whole generated power. Thus, safety mechanisms must be activated to remove the excess of active power production that may produce dc-link overvoltage and overcurrent disconnection. A method to avoid these problems is the active power curtailment. It comprises the retail of the active power according to specific requirements by means of auxiliary systems such as dc-link voltage limiter units or by detuning the MPPT operation point [27], [28].

On the other hand, if the calculated reference currents do not exceed the maximum rated current during the sag, the inverter power capability is not completely exploited. In this situation, reactive power injection could be considered to reach the maximum rated current and maximize the inverter power capability.

To solve the aforementioned issues during voltage sags (i.e., to avoid active power oscillations, to avoid inverter tripping due to over current, and to inject the reactive power when is possible), a new current control strategy that maximizes the inverter power capabilities is proposed below.

B. Proposed Control Strategy

To achieve the previously mentioned control objectives, a set of flexible reference currents are needed. Thus, based on [9], a new set of reference currents is defined as

$$i_\alpha^*(p) = \frac{2}{3} \frac{k_p^+ v_\alpha^+ + k_p^- v_\alpha^-}{k_p^+ (V^+)^2 + k_p^- (V^-)^2} P^* \quad (12)$$

$$i_\beta^*(p) = \frac{2}{3} \frac{k_p^+ v_\beta^+ + k_p^- v_\beta^-}{k_p^+ (V^+)^2 + k_p^- (V^-)^2} P^* \quad (13)$$

$$i_\alpha^*(q) = \frac{2}{3} \frac{k_q^+ v_\beta^+ + k_q^- v_\beta^-}{k_q^+ (V^+)^2 + k_q^- (V^-)^2} Q^* \quad (14)$$

$$i_\beta^*(q) = -\frac{2}{3} \frac{k_q^+ v_\alpha^+ + k_q^- v_\alpha^-}{k_q^+ (V^+)^2 + k_q^- (V^-)^2} Q^* \quad (15)$$

where k_p^+ , k_p^- , k_q^+ , and k_q^- are the control parameters to balance appropriately the positive and negative sequences. These parameters can take any values in the range 0 to 1, which give rise to multiple injection strategies. For instance, the simple injection strategy represented by (10) and (11) can be implemented with the proposed reference currents by selecting the control parameter as $k_p^+ = k_q^+ = 1$ and $k_p^- = k_q^- = Q^* = 0$.

Thus, based on (12)–(15), a control strategy that determines adequately the power references (P^* , Q^*) to fulfill the proposed control objectives is presented. The operation of the proposed control strategy can be described by the algorithm shown in Fig. 2. In this figure, the generated active power reference P_G is obtained from the dc-link voltage regulator. The positive- and negative-voltage sequences are obtained from the sequence

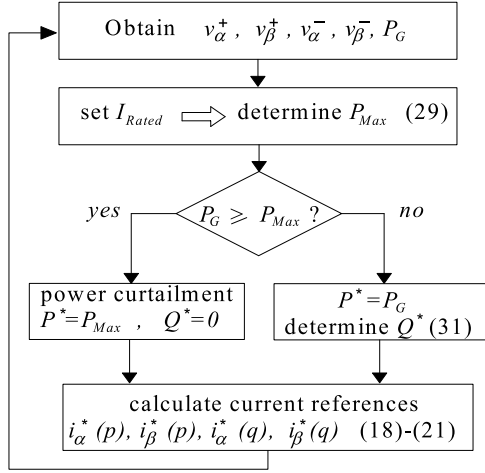


Fig. 2. Flux diagram of the proposed control strategy.

extractor which let to determine the sag characteristics [29], [30]. Next, the maximum allowable active power P_{Max} is calculated considering the value of the maximum rated current that the VSI can provide (I_{Rated}) and $Q^* = 0$. Afterward, P_{Max} is compared with P_G to determinate the suitable control action. If P_G is higher than P_{Max} , the strategy applies power curtailment to avoid exceeding I_{Rated} . Consequently, a new value to the active power reference has to be set as $P^* = P_{Max}$ and the reactive power reference is maintained as $Q^* = 0$. On the other hand, if P_G is lower than P_{Max} , then, the inverter maximum rated current is not surpassed and, therefore, some amount of the reactive power can be injected up to reach I_{Rated} . In this case, the reactive power reference Q^* is calculated considering I_{Rated} and the generated power P_G . Finally, the reference currents are computed with the corresponding values of active and reactive power references. The selection of the control parameter and the development of the mathematical expressions that allows the online determination of P_{Max} and Q^* will be shown in Section IV.

IV. THEORETICAL APPROACH TO THE CONTROL STRATEGY

The purpose of this section is to develop the mathematical expressions that support the statements of the proposed control strategy. Furthermore, the effects that the proposed reference currents and control parameters cause in the instantaneous active and reactive power are presented.

A. Determining Maximum Injected Current

To fulfill the control objective of avoiding active power oscillations, the control parameters are selected as

$$k_p^- = -k_p^+ \quad (16)$$

$$k_q^+ = k_q^- \quad (17)$$

The achievement of this objective will be validated theoretically in Section IV-C and experimentally in Section V. Additionally, thanks to (16) and (17), the proposed reference currents

(12)–(15) become simplified and normalized as follows:

$$i_\alpha^*(p) = \frac{2}{3} \frac{v_\alpha^+ - v_\alpha^-}{(V^+)^2 - (V^-)^2} P^* \quad (18)$$

$$i_\beta^*(p) = \frac{2}{3} \frac{v_\beta^+ - v_\beta^-}{(V^+)^2 - (V^-)^2} P^* \quad (19)$$

$$i_\alpha^*(q) = \frac{2}{3} \frac{v_\beta^+ + v_\beta^-}{(V^+)^2 + (V^-)^2} Q^* \quad (20)$$

$$i_\beta^*(q) = -\frac{2}{3} \frac{v_\alpha^+ + v_\alpha^-}{(V^+)^2 + (V^-)^2} Q^* \quad (21)$$

Then, using (1), (2), (18)–(21), the peak amplitude of the natural frame phase currents can be easily calculated by applying the inverse-Clarke transformation to (8) and (9). The resulting amplitudes depend on the sag characteristics, and the active and reactive power references as

$$I_a = \frac{2}{3} \sqrt{((V^+)^2 - 2V^+V^- \cos(\delta) + (V^-)^2)} A \quad (22)$$

$$I_b = \frac{2}{3} \sqrt{((V^+)^2 - 2V^+V^- \cos(\delta - 2/3\pi) + (V^-)^2)} A \quad (23)$$

$$I_c = \frac{2}{3} \sqrt{((V^+)^2 - 2V^+V^- \cos(\delta + 2/3\pi) + (V^-)^2)} A \quad (24)$$

where

$$A = \left(\frac{P^*}{(V^+)^2 - (V^-)^2} \right)^2 + \left(\frac{Q^*}{(V^+)^2 + (V^-)^2} \right)^2 \quad (25)$$

From (22)–(24), it can be clearly seen that the phase with the maximum current is related with the minimum value of the corresponding cosine function

$$\cos_{\min} = \min \{ \cos(\delta), \cos(\delta - 2/3\pi), \cos(\delta + 2/3\pi) \} \quad (26)$$

Then, measuring the sag characteristics (V^+, V^-, δ) and knowing the active and reactive power references, the maximum phase current amplitude can be easily determined as

$$I_{Max} = \frac{2}{3} \sqrt{((V^+)^2 - 2V^+V^- \cos_{\min} + (V^-)^2)} A \quad (27)$$

where I_{Max} is the maximum output current that the VSI will provide.

To avoid inverter damage or disconnection by the overcurrent, I_{Max} must be limited to the VSI-maximum-rated current by means of the following condition:

$$I_{Max} \leq I_{Rated} \quad (28)$$

B. Determining Maximum Active and Reactive Power

The maximum power that the VSI can deliver during the sag must be determined considering (28). Also, variations in the generated power due to different environmental conditions must be considered. Therefore, high- and low-power production scenarios can be studied during the occurrence of grid faults.

Scenario 1 (High power generation): In this case, I_{Rated} could be surpassed due to the generated power P_G . In this situation, the source is unable to inject the whole generated power, and active power curtailment is necessary. Then, the maximum active power that can be injected into the grid during the sag can be

determined by using $I_{\text{Max}} = I_{\text{Rated}}$, $P^* = P_{\text{Max}}$, and $Q^* = 0$ in (27), and solving the resulting expression for P_{Max}

$$P_{\text{Max}} = \frac{3}{2} \frac{I_{\text{Rated}}}{\sqrt{B}} ((V^+)^2 - (V^-)^2) \quad (29)$$

where

$$B = (V^+)^2 - 2V^+V^- \cos_{\text{min}} + (V^-)^2. \quad (30)$$

In this case, the active and reactive power references are $P^* = P_{\text{Max}}$ and $Q^* = 0$.

Scenario 2 (Low power generation): In this case, the generated power P_G is lower than P_{Max} , and the inverter maximum rated current cannot be reached, then, some amount of the reactive power can be injected to increase the VSI output currents up to its maximum value in order to support the grid. Under this situation, the reactive power reference can be determined by using $I_{\text{Max}} = I_{\text{Rated}}$ and $P^* = P_G$ in (27) and solving the resulting expression for Q^*

$$Q^* = \sqrt{\frac{2.25I_{\text{Rated}}^2}{B} - \left(\frac{P_G}{(V^+)^2 - (V^-)^2}\right)^2} ((V^+)^2 + (V^-)^2). \quad (31)$$

In this case, the active power reference is $P^* = P_G$.

It is worth mentioning that (29) and (31) are simple and compact expressions that facilitate the application of the proposed control strategy. As far as author's knowledge refers, these expressions have not been reported previously in the literature, thus, together with the flux diagram shown in the Fig. 2, these constitute the two main theoretical contributions of this paper.

C. Determining Power Oscillations Components

During voltage sag, the instantaneous active and reactive powers injected by the VSI can be decomposed in the following expressions:

$$p = P^+ + P^- + \tilde{P} \quad (32)$$

$$q = Q^+ + Q^- + \tilde{Q} \quad (33)$$

where P^+ , Q^+ , P^- , Q^- , \tilde{P} , and \tilde{Q} represents the positive and negative components and the oscillating terms of the active and reactive power, respectively.

By inserting (1)–(2) and (12)–(15) into (6) and (7), (32) and (33) can be developed as a function of V^+ , V^- , δ , and the control parameters as

$$P^+ = \frac{k_p^+(V^+)^2}{k_p^+(V^+)^2 + k_p^-(V^-)^2} P^* \quad (34)$$

$$P^- = \frac{k_p^-(V^-)^2}{k_p^+(V^+)^2 + k_p^-(V^-)^2} P^* \quad (35)$$

$$\begin{aligned} \tilde{P} = & \frac{(k_p^+ + k_p^-)V^+V^- \cos(2\omega t - \delta)}{k_p^+(V^+)^2 + k_p^-(V^-)^2} P^* \\ & + \frac{(k_p^+ - k_p^-)V^+V^- \sin(2\omega t - \delta)}{k_p^+(V^+)^2 + k_p^-(V^-)^2} Q^* \end{aligned} \quad (36)$$

$$Q^+ = \frac{k_q^+(V^+)^2}{k_q^+(V^+)^2 + k_q^-(V^-)^2} Q^* \quad (37)$$

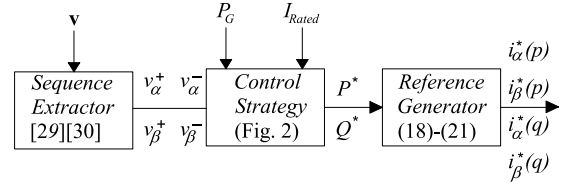


Fig. 3. Block diagram of the proposed control scheme.

$$Q^- = \frac{k_q^-(V^-)^2}{k_q^+(V^+)^2 + k_q^-(V^-)^2} Q^* \quad (38)$$

$$\begin{aligned} \tilde{Q} = & \frac{(k_q^+ + k_q^-)V^+V^- \cos(2\omega t - \delta)}{k_q^+(V^+)^2 + k_q^-(V^-)^2} Q^* \\ & - \frac{(k_q^+ - k_q^-)V^+V^- \sin(2\omega t - \delta)}{k_q^+(V^+)^2 + k_q^-(V^-)^2} P^*. \end{aligned} \quad (39)$$

Then, by replacing the proposed control parameters ($k_p^- = -k_p^+$ and $k_q^+ = k_q^-$) in (34)–(39), the resulting instantaneous active and reactive power can be written as

$$p = P^* \quad (40)$$

$$\begin{aligned} q = & Q^* + \frac{2V^+V^- \cos(2\omega t - \delta)}{(V^+)^2 + (V^-)^2} Q^* \\ & - \frac{2V^+V^- \sin(2\omega t - \delta)}{(V^+)^2 - (V^-)^2} P^*. \end{aligned} \quad (41)$$

As it can be seen from (40) and (41), the oscillation of the injected active power is removed completely, which brings benefits to the dc-link performance. On the other hand, the reactive power has oscillations at twice the line frequency, but ensuring a mean value Q^* .

D. Proposed Control Scheme

A simplified diagram of the control proposal is shown in Fig. 3. The inputs of the controller are the measured phase voltages \mathbf{v} at the PCC, and the generated power P_G provided by the dc-link voltage controller. Voltage vector \mathbf{v} is converted into SRF values by means of Clarke transformation. Then, voltages v_α and v_β are decomposed into symmetric components using a sequence extractor. The core of the controller is the control strategy block, whose operation has been described by Fig. 2. It uses the information provided by the sequence extractor and the inputs, P_G and I_{Rated} , to calculate the power references necessary to implement the proposed reference currents.

V. EXPERIMENTAL RESULTS

Fig. 4 shows a diagram of the experimental setup. An experimental prototype rated at 2.3 kVA was built using a SEMIKRON three-leg bridge, an LCL power filter, a three-phase power transformer, and a local load. A TMS320F28335 floating point digital signal processor is used as the control platform. The DG source behavior is emulated using an AMRELS-SPS1000 dc source. The utility grid is emulated by means of a programmable three-phase Pacific AMX-360 ac source connected to the PCC. The sequence extractor is implemented

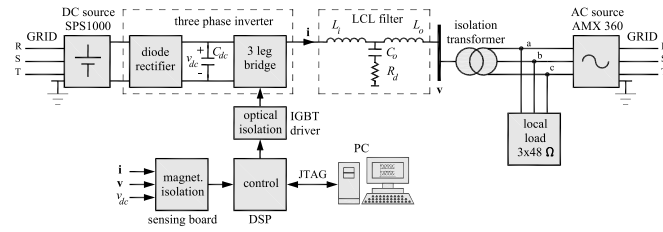


Fig. 4. Diagram of the experimental setup.

TABLE I
SYSTEM PARAMETERS

Quantity	Symbol	Nominal value
Nominal rated power (base power)	S_b	2.3 kVA
Generated active power	P_G	300, 900, and 1300 W
Nominal grid voltage	V_g	110 Vrms
Rated current amplitude	I_{Rated}	10 A
Nominal grid frequency	f_o	60 Hz
DC-link voltage	V_{dc}	350 V
DC-link capacitor	C_{dc}	1.5 mF
LCL inverter-side inductances	L_i	5 mH
LCL filter capacitors	C_o	1.5 μ F
LCL damping resistors	R_d	68 Ω
LCL output-side inductances	L_o	2 mH
Sampling/Switching frequency	f_s	10 kHz

with generalized integrators [29], [30]. The current controller consists of proportional-resonant controllers [31]. Table I lists the parameter values for both the inverter and the controller.

Throughout this paper, two power production scenarios have been considered: high and low. However, an additional medium production scenario has been also included in this section, in order to highlight the flexible characteristic of the proposed control scheme. Then, three different power production tests have been considered to obtain experimental results: low-, medium-, and high-production scenarios.

A variable-profile voltage sag has been programmed in the ac source to evaluate the behavior of the system. The programmed sag in three different power production tests will follow the same sequential behavior. First, during 0.1 s, the grid voltages are roughly balanced with the following rms voltages: 1.018, 1.025, and 1.021 p.u. Then, at $t = 0.1$ s, the sag appears and two phases voltages drop well below 0.7 p.u., with a minimum of 0.58 p.u. Afterward, during 0.25 s (from $t = 0.1$ s to $t = 0.35$ s) the sag profile changes slightly, in order to show the behavior of the control strategy. Finally, at time $t = 0.35$ s, the sag is cleared and the dropped voltages begin to return to its presag values. Fig. 5 shows the PCC line-to-neutral phase voltages during the sag and its rms per unit values.

A. Low Active Power Injection Scenario

Fig. 6 shows the instantaneous active and reactive power during the fault considering $P_G = 300$ W, i.e., a low-production scenario. The mean value of the active power is 300 W for the duration of the test (see the line depicted in blue). In red line, the maximum active power P_{Max} that could be injected without surpassing I_{Rated} is depicted in the figure. Then, when the sag begins, the proposed current controller calculates on-line P_{Max} for this specific fault. Observe that P_{Max} is reduced from 2.3 kW

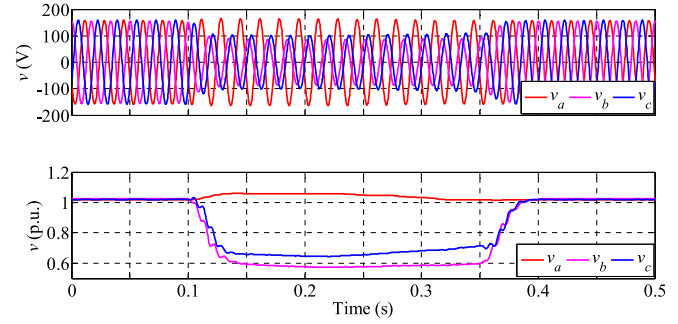
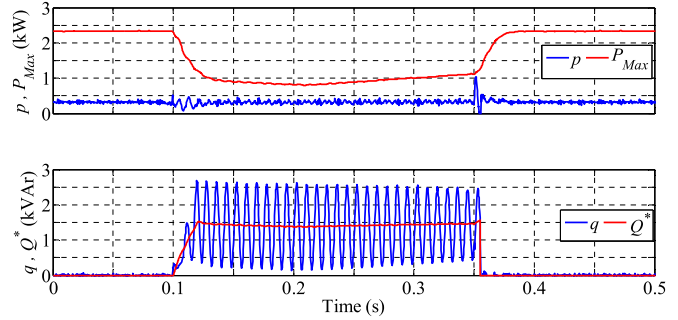
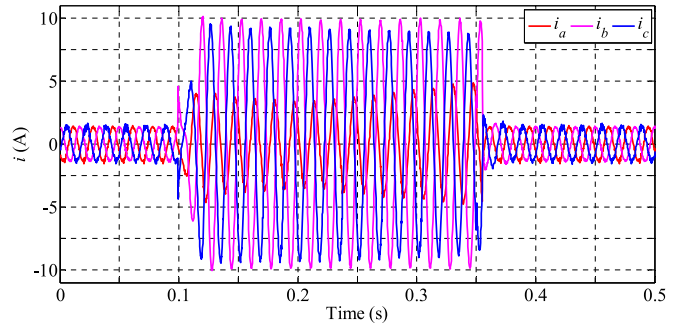


Fig. 5. Experimental PCC phase voltages during the sag (top), and its rms values (bottom).

Fig. 6. Experimental results for low injection scenario, $P_G = 300$ W. Top: measured active power, p , and maximum power P_{Max} . Bottom: measured reactive power, q , and reference reactive power Q^* .Fig. 7. Experimentally measured line currents for low injection scenario, $P_G = 300$ W.

to a minimum value of 800 W during the sag. As it can be seen, the power produced by the system never reaches P_{Max} , thus $P^* = P_G$ during the entire test. Under this condition, the inverter is able to provide some reactive power till the maximum-rated current I_{Rated} of the inverter is reached. The measured mean value of the injected reactive power is almost 1.4 kVar during the sag, clearly following its reference value Q^* . When the sag takes place, the system becomes unbalanced and an oscillation at twice the line frequency appears in the reactive power. In the case of the active power, observe that thanks to the selection of the control parameters (16), (17), its oscillations have been avoided as desired.

Fig. 7 shows the injected currents during the test. After 0.02 s of the sag appearance, the objective of injecting the maximum allowed current is fulfilled in one phase. Note that the amplitudes

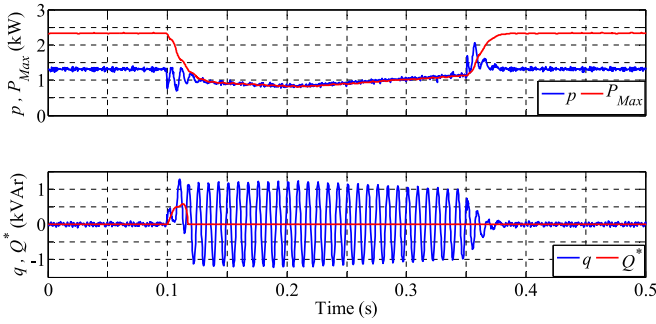


Fig. 8. Experimental results for high injection scenario, $P_G = 1300$ W. Top: measured active power, p , and maximum power P_{Max} . Bottom: measured reactive power, q , and reference reactive power Q^* .

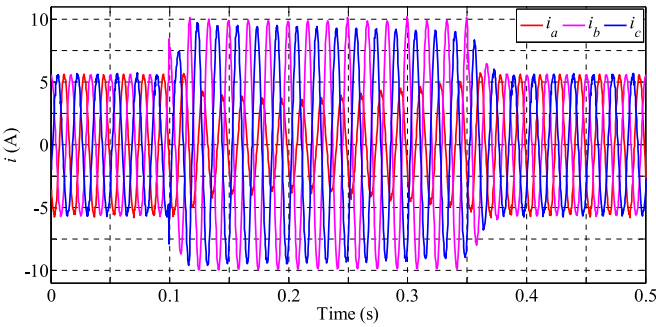


Fig. 9. Experimentally measured line currents for high injection scenario, $P_G = 1300$ W.

of the other phase currents are changing continuously due to the variable profile of the voltage sag and never exceed the maximum-rated current.

B. High Active Power Injection Scenario

Fig. 8 shows the instantaneous active and reactive powers during the fault considering $P_G = 1300$ W, i.e., a high-production scenario. The mean value of the injected active power is 1300 W before and after of the sag, $P^* = P_G$. On the other hand, as it can be observed, the maximum active power P_{Max} is surpassed by the produced power during the sag. Under this condition, the power production must be curtailed to avoid overcurrent and disconnection. During the sag, the active power reference is limited to P_{Max} , i.e., $P^* = P_{Max}$. Thus, in this test, no reactive power can be provided since the maximum output current of the inverter I_{Rated} has been reached. It is important to note that the voltage sequences detector has a one grid-cycle settling-time response, which introduces a delay in the reactive power reference Q^* calculation. This effect can be observed at the beginning of the sag, when the reactive power injection is not zero and reaches 500 VAr during one grid cycle. However, after this small time interval, the reactive power reference reaches its expected value $Q^* = 0$ VAr (zero mean value). Also, an oscillation in the reactive power at twice the line frequency is observed, which corroborates the prediction of the previous analysis. Fig. 9 shows the injected currents during the test. After 0.015 s of the sag appearance, the objective of injecting the maximum allowed current is fulfilled.

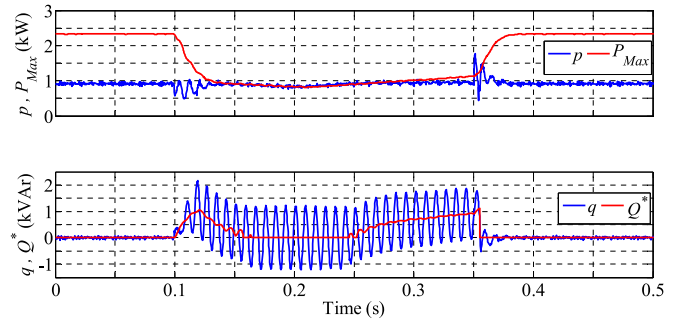


Fig. 10. Experimental results for medium injection scenario, $P_G = 900$ W. Top: measured active power, p , and maximum power P_{Max} . Bottom: measured reactive power, q , and reference reactive power Q^* .

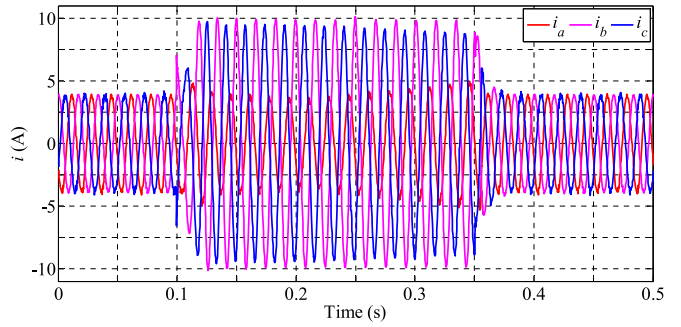


Fig. 11. Experimentally measured line currents for medium injection scenario, $P_G = 900$ W.

C. Medium Active Power Injection Scenario

Fig. 10 shows the instantaneous active and reactive power during the fault considering $P_G = 900$ W, i.e., a medium-production scenario. The mean value of the injected active power is 900 W before and after the sag, $P^* = P_G$. A combination of the previous scenarios can be observed in Fig. 10, from the beginning of the sag until 0.15 s and from 0.25 s to the end of the sag, in which the active power generated by the system is below P_{Max} and some reactive power can be injected. Among these two intervals, P_{Max} is surpassed and the power production must be curtailed ($P^* = P_{Max}$) to avoid overcurrents. Fig. 11 shows the injected currents during this test. This test reveals the excellent dynamic properties of the proposed control strategy which provide smooth transitions between the operation modes (i.e., active power curtailment and reactive power injection).

D. Supporting Different Types of Voltages Sags

A complete set of simulations has been carried out to further demonstrate the effectiveness of the control proposal under any type of voltage sag. The system with parameters described in Table I has been simulated under three types of sags, characterized by its positive- and negative-sequence voltages, V^+ and V^- , and the sequence phase angle δ [9], [23]. Also, a positive-gradient change in the active power P_G has been programmed during the sag, beginning at $t = 0.2$ s, to demonstrate the capability of the proposed strategy to react against transient generation conditions.

Fig. 12 shows the simulation results when the system is perturbed by a type-II sag ($\delta = 10^\circ$). The mean value of the injected

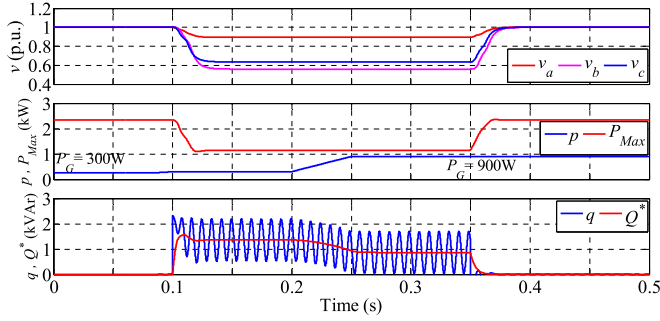


Fig. 12. Simulation waveforms for type-II sag ($V^+ = 0.68$, $V^- = 0.22$, $\delta = 10^\circ$). Top: PCC rms phase voltages. Middle: generated active power, p , and maximum power P_{Max} . Bottom: measured reactive power, q , and reference reactive power Q^* .

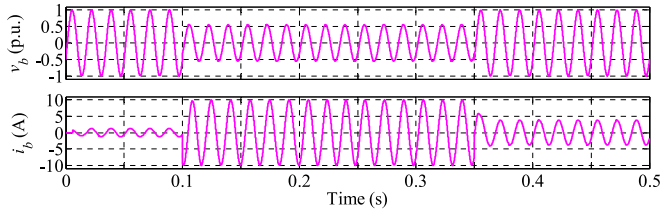


Fig. 13. Phase b voltage and current during the type II sag. Top: PCC line-to-neutral voltage. Bottom: phase current.

active power is 300 W before the sag and 900 W after the sag due to the programmed active power change. As it can be seen, the generated power never reaches P_{Max} , thus, $P^* = P_G$ during the entire simulation. Under this condition, the inverter is able to provide some reactive power till the inverter maximum-rated current I_{Rated} is reached. Note that the reactive power adapts its profile online to the changes produced in the generated power in order to safely maintain the inverter-rated current controlled at its maximum value.

Fig. 13 depicts the line-to-neutral voltage at phase b and the corresponding current during the type-II sag. Observe that the i_b peak current change according to the delivered power. Before the sag, the peak current is low (approximately 1 A). During the sag, it reaches I_{Rated} because v_b is the most dropped phase voltage. After the sag, the peak current decrease up to approximately 4 A due to the increment in the active power. Note that the maximum rated current is not surpassed at any time.

Fig. 14 shows the simulations for the type I sag ($\delta = 280^\circ$). An active power change has been programmed from 300 W up to 1300 W. In this test, the injection of the active power is curtailed by the controller approximately at $t = 0.23$ s, once the generated power reaches P_{Max} . Thus, from this point till the sag is cleared, $P^* = P_{Max}$. After the sag, the delivered active power increases up to 1300 W. During this test, it is verified that the inverter provides reactive power meanwhile the generated power is below the limit P_{Max} .

The well performance of the system during type-III sag is similar to that obtained in previous tests, as shown in Fig. 15. In this case, the change in the generated power has been programmed from 300 W up to 2000 W. Thus, the system is able to deliver this maximum value of the active power once the sag is cleared. Since the voltage droop is balanced in the three phases,

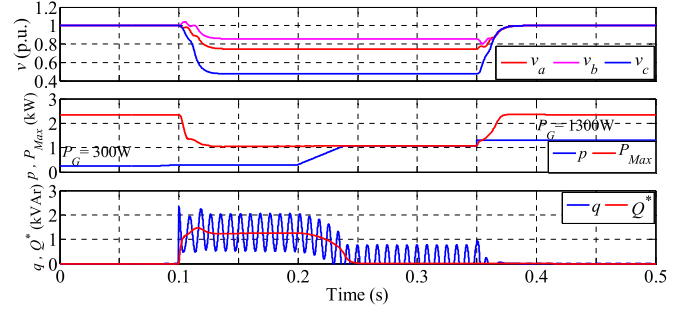


Fig. 14. Simulation waveforms for type-I sag ($V^+ = 0.68$, $V^- = 0.22$, $\delta = 280^\circ$). Top: PCC rms phase voltages. Middle: generated active power, p , and maximum power P_{Max} . Bottom: measured reactive power, q , and reference reactive power Q^* .

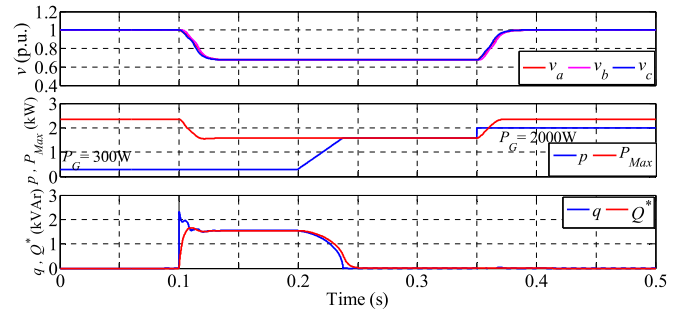


Fig. 15. Simulation waveforms for type-III sag. ($V^+ = 0.68$, $V^- = 0.22$, $\delta = 0^\circ$). Top: PCC rms phase voltages. Middle: generated active power, p , and maximum power P_{Max} . Bottom: measured reactive power, q , and reference reactive power Q^* .

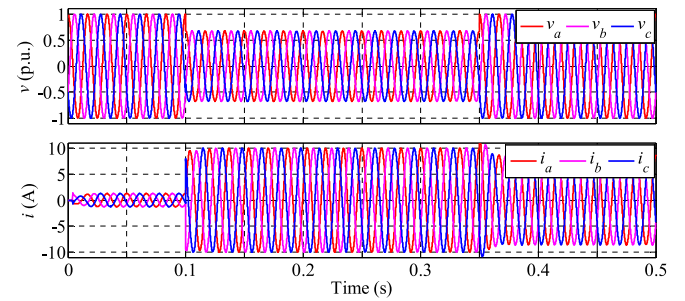


Fig. 16. Voltage and phase currents waveforms during the type-III sag. Top: PCC phase voltages. Bottom: phase currents.

the output currents are also balanced with maximum amplitudes of 10 A as shown in Fig. 16.

The simulations results obtained during the tests verify the outstanding dynamics properties of the proposed strategy that is able to handle both different types of sags, and the changes in the generated power. Table II summarizes the results for the three simulation tests. Note that the maximum current is 10 A in only one phase for type-I and type-II sags, while in the type-III sag, the current amplitudes are 10 A in all the phases.

E. Discussion on the Benefits of the Proposed Strategy

The performance of VSI under voltage sags has been widely investigated. However, the best strategy is still an open research

TABLE II
PEAK CURRENT VALUES DURING DIFFERENT SAGS

Sag type	I	II	III
Sag	$V^+ = 0.68$	$V^+ = 0.68$	$V^+ = 0.68$
Characteristics	$V^- = 0.22$ $\delta = 280^\circ$	$V^- = 0.22$ $\delta = 10^\circ$	$V^- = 0$ $\delta = 0^\circ$
i_a (A)	7.69	5.51	10.00
i_b (A)	6.01	10.00	10.00
i_c (A)	10.00	9.32	10.00

TABLE III
COMPARISON WITH PREVIOUS STRATEGIES

Strategy	Deliver to the grid	Peak current limitation	Injected current THD	Reduce p oscillation	Control Complexity
[12]	only P	No	High	No	Low
[13], [14]	only Q	Yes	Low	No	Low
[16]	P and Q	Yes	Low	No	High
[17]	P and Q	Yes	Low	Yes	High
Proposal	P and Q	Yes	Low	Yes	Low

topic and depends on many aspects such as grid stiffness, DG-rated power, type of prime mover, type of sag, external requirements, etc. The control strategy presented in this paper is based on a flexible reference current generator that can be adjusted by means of two control parameters to obtain different results in terms of power quality, balance among positive and negative sequences, active and reactive power injection characteristics, among others. In fact, it can reproduce previous injection strategies by proper selection of the control parameters.

One of the contributions of this paper is a particular selection of the control parameter which permits to preserve one remarkable feature of previous strategies such as the mitigation of active power oscillation. Furthermore, thanks to the proposed parameter selection, the referent current generator (see (12)–(15)) turns into a simple and normalized structure that permits to develop two simple and compact expressions (see (29) and (31)). It is worth mentioning that these expressions incorporate the peak current limitation function and facilitate the devise of the proposed control strategy as shown in Fig. 2. The proposed strategy gives priority to the injection of active power which matches correctly with the actual PV GCs requirements. Furthermore, under sag situation, a reactive power reference is online computed based on the remaining VSI current capacity. This property permits to support the grid during contingencies and, at the same time, it protects the inverter against overcurrent.

The proposal shares important features with some previous strategies such as peak current limitation and mitigation of active power oscillation. Furthermore, it reduces the implementation complexity integrating these functionalities in two compact expressions. In addition, the proposed strategy provides outstanding dynamic behavior that permits to obtain smooth transitions under active power variations and also during changes in the operation modes (i.e., active power curtailment and reactive power injection). To summarize the discussion, Table III compares the main features of the proposal and previous strategies.

VI. CONCLUSION

This paper has presented an LVRT control strategy that maximizes the power capabilities of distributed PV inverters under voltage sag. By means of the proposed flexible current injection strategy, two main objectives have been achieved. First, to safely maintain the injected currents at the maximum rated value, independently of the sag profile and generated power, and second, to avoid oscillations in the injected active power. Both objectives contribute to improve the grid stability and ensure an optimized use of the whole VSI power capability, improving the quality of the injected power. The effectiveness of the proposed control strategy has been validated by a comprehensive set of simulation and experimental results.

REFERENCES

- [1] F. Blaabjerg, R. Teodorescu, M. Liserre, and A. V. Timbus, "Overview of control and grid synchronization for distributed power generation systems," *IEEE Trans. Ind. Electron.*, vol. 53, no. 5, pp. 1398–1409, Oct. 2006.
- [2] F. Blaabjerg, Z. Chen, and S. B. Kjaer, "Power electronics as efficient interface in dispersed power generation systems," *IEEE Trans. Power Electron.*, vol. 19, no. 5, pp. 1184–1194, Sep. 2004.
- [3] S. Martin-Martinez, E. Gomez-Lazaro, A. Molina-Garcia, A. Molina-Garcia, A. Viguera-Rodriguez, M. Milligan, and E. Muljadi, "Participation of wind power plants in the Spanish power system during events," in *Proc. IEEE Power Energy Soc. General Meeting*, 2012, pp. 1–8.
- [4] (2008 Oct.). Offprint of the Operation Procedure O.P. 12.2: Technical requirements for wind power and photovoltaic installations and any generating facilities whose technology does not consist on a synchronous generator directly connected to the grid, Asociación Empresarial Eólica. [Online]. Available: www.aeolica.org
- [5] M. Altin, O. Goksu, R. Teodorescu, P. Rodriguez, B.-B. Jensen, and L. Helle, "Overview of recent grid codes for wind power integration," in *Proc. 12th Int. Conf. Optimization Electr. Electron. Equip.*, May 2010, pp. 1152–1160.
- [6] *Characteristics of the Utility Interface for Photovoltaic Systems*, IEC Standard 61727, 2004.
- [7] S. Alepuz, S. Busquets-Monge, J. Bordonau, J. Martinez-Velasco, C. Silva, J. Pont, and J. Rodriguez, "Control strategies based on symmetrical components for grid-connected converters under voltage dips," *IEEE Trans. Ind. Electron.*, vol. 56, no. 6, pp. 2162–2173, Jun. 2009.
- [8] F. Wang, J. L. Duarte, and M. A. M. Hendrix, "Pliant active and reactive power control for grid-interactive converters under unbalanced voltage dips," *IEEE Trans. Power Electron.*, vol. 26, no. 5, pp. 1511–1521, May 2011.
- [9] A. Camacho, M. Castilla, J. Miret, J. C. Vasquez, and E. Alarcon-Gallo, "Flexible voltage support control for three phase distributed generation inverters under grid fault," *IEEE Trans. Ind. Electron.*, vol. 60, no. 4, pp. 1429–1441, Apr. 2013.
- [10] J. Miret, A. Camacho, M. Castilla, L. García de Vicuña, and J. Matas, "Control scheme with voltage support capability for distributed generation inverters under-voltage sags," *IEEE Trans. Power Electron.*, vol. 28, no. 11, pp. 5252–5262, Nov. 2013.
- [11] A. Camacho, M. Castilla, J. Miret, R. Guzman, and A. Borrell, "Reactive power control for distributed generation power plants to comply with voltage limits during grid faults," *IEEE Trans. Power Electron.*, vol. 29, no. 11, pp. 2624–2634, Nov. 2014.
- [12] J. Miret, M. Castilla, A. Camacho, L. García de Vicuña, and J. Matas, "Control scheme for photovoltaic three-phase inverters to minimize peak currents during unbalanced grid-voltage sags," *IEEE Trans. Power Electron.*, vol. 27, no. 10, pp. 4262–4271, Oct. 2012.
- [13] P. Rodriguez, A. Luna, J. Hermoso, I. Etxebarria-Otadui, R. Teodorescu, and F. Blaabjerg, "Current control method for distributed generation power generation plants under grid fault conditions," in *Proc. IEEE 37th Annu. Conf. Ind. Electron. Soc.*, Nov. 2011, pp. 1262–1269.
- [14] P. Rodriguez, G. Medeiros, A. Luna, M. Cavalcanti, and R. Teodorescu, "Safe current injection strategies for a STATCOM under asymmetrical grid faults," in *Proc. IEEE Energy Convers. Congr. Expo.*, Sep. 2010, pp. 3929–3935.

- [15] J. Suul, A. Luna, P. Rodríguez, and T. Undeland, "Virtual-flux-based voltage-sensor-less power control for unbalanced grid conditions," *IEEE Trans. Power Electron.*, vol. 27, no. 9, pp. 4071–4087, Sep. 2012.
- [16] C.-T. Lee, C.-W. Hsu, and P.-T. Cheng, "A low-voltage ride-through technique for grid-connected converters of distributed energy resources," *IEEE Trans. Ind. Appl.*, vol. 47, no. 4, pp. 1821–1832, Jul. 2011.
- [17] A. Camacho, M. Castilla, J. Miret, A. Borrell, and L. García de Vicuña, "Active and reactive power strategies with peak current limitation for distributed generation inverters during unbalanced grid faults," *IEEE Trans. Ind. Electron.*, vol. 62, no. 3, pp. 1515–1525, Mar. 2015.
- [18] M. Liserre, F. Blaabjerg, and S. Hansen, "Design and control of an LCL filter-based three-phase active rectifier," *IEEE Trans. Ind. Appl.*, vol. 41, no. 5, pp. 1281–1291, Sep./Oct. 2005.
- [19] E. Figueres, G. Garcera, J. Sandia, F. Gonzalez-Espin, and J. C. Rubio, "Sensitivity study of the dynamics of three-phase photovoltaic inverters with an LCL grid filter," *IEEE Trans. Ind. Electron.*, vol. 56, no. 3, pp. 706–717, Mar. 2009.
- [20] A.K. Abdelsalam, A. M. Massoud, S. Ahmed, and P. N. Enjeti, "High-performance adaptive perturb and observe MPPT technique for photovoltaic-based microgrids," *IEEE Trans. Power Electron.*, vol. 26, no. 4, pp. 1010–1021, Apr. 2011.
- [21] M. Mohseni, S. M. Islam, and M. A. S. Masoum, "Impacts of voltage sags on DFIG-based wind turbines considering phase-angle jump, voltage recovery, and sag parameters," *IEEE Trans. Power Electron.*, vol. 26, no. 5, pp. 1587–1598, May 2011.
- [22] M. H. J. Bollen, "Algorithms for characterizing measured three-phase unbalanced voltage dips," *IEEE Trans. Power Del.*, vol. 18, no. 3, pp. 937–944, Jul. 2003.
- [23] V. Ignatova, P. Granjon, and S. Bacha, "Space vector method for voltage dips and swells analysis," *IEEE Trans. Power Del.*, vol. 24, no. 4, pp. 2054–2061, Oct. 2009.
- [24] A. Yazdani, and R. Iravani, *Voltage-Sourced Converters in Power Systems*. Hoboken, NJ, USA: Wiley, 2010.
- [25] H. Akagi, Y. Kanazawa, and A. Nabae, "Instantaneous reactive power compensator comprising switching devices without energy storage components," *IEEE Trans. Ind. Appl.*, vol. IA-20, no. 3, pp. 625–630, May 1984.
- [26] P. Rodríguez, A. V. Timbus, R. Teodorescu, M. Liserre, and F. Blaabjerg, "Flexible active power control of distributed power generation systems during grid faults," *IEEE Trans. Ind. Electron.*, vol. 54, no. 5, pp. 2583–2592, Oct. 2007.
- [27] R. Tonkoski, L. A. C. Lopes, and T. H. M. El-Fouly, "Coordinated active power curtailment of grid connected PV inverters for overvoltage prevention," *IEEE Trans. Sustainable Energy*, vol. 2, no. 2, pp. 139–147, Apr. 2011.
- [28] J. F. Conroy and R. Watson, "Low-voltage ride-through of a full converter wind turbine with permanent magnet generator," *IET Renew. Power Gener.*, vol. 1, no. 3, pp. 182–189, Sep. 2007.
- [29] J. Matas, M. Castilla, J. Miret, L. García de Vicuña, and R. Guzman, "An adaptive pre-filtering method to improve the speed/accuracy trade-off of voltage sequence detection methods under adverse grid conditions," *IEEE Trans. Ind. Electron.*, vol. 61, no. 5, pp. 2139–2151, May 2014.
- [30] F. Rodríguez, E. Bueno, M. Aredes, L. Rolim, F. Neves, and M. Cavalcanti, "Discrete-time implementation of second order generalized integrators for grid converters," in *Proc. IEEE 34th Annu. Conf. Ind. Electron.*, Nov. 2008, pp. 176–181.
- [31] D. N. Zmood, D. G. Holmes, and G. H. Bode, "Frequency-domain analysis of three-phase linear current regulators," *IEEE Trans. Ind. Appl.*, vol. 37, no. 2, pp. 601–610, Mar./Apr. 2001.



Jorge Luis Sosa received the B.S. and M.S. degrees in electrical engineering from the Universidad de Los Andes, Mérida, Venezuela, in 1993 and 1997, respectively, and the Ph.D. degree from the Technical University of Catalonia, Barcelona, Spain, in 2007.

Since 1999, he has been a Professor with the Scientific Instrumentation Laboratory, Universidad de los Andes, Mérida, Venezuela, where he teaches courses in electronics. His current research interests include nonlinear control of power converters, distributed power systems, uninterruptible power systems, and

power electronics.



Miguel Castilla received the B.S., M.S., and Ph.D. degrees in telecommunication engineering from the Technical University of Catalonia, Barcelona, Spain, in 1988, 1995, and 1998, respectively.

Since 2002, he has been an Associate Professor in the Department of Electronic Engineering, Technical University of Catalonia, where he teaches courses on analog circuits and power electronics. His research interests are in the areas of power electronics, nonlinear control, and renewable energy systems.



Jaume Miret (M'98) received the B.S. degree in telecommunications, the M.S. degree in electronics, and the Ph.D. degree in electronics from the Universitat Politècnica de Catalunya, Barcelona, Spain, in 1992, 1999, and 2005, respectively.

From 1993 to 2011, he was an Assistant Professor in the Department of Electronic Engineering, Universitat Politècnica de Catalunya, Spain, where he has been an Associate Professor since 2011 and teaches courses on digital design and circuit theory. His research interests include dc-to-ac converters, active

power filters, and digital control.



José Matas received the B.S., M.S., and Ph.D. degrees in telecommunications engineering from the Technical University of Catalonia, Barcelona, Spain, in 1988, 1996, and 2003, respectively.

From 1988 to 1990, he was an Engineer in a consumer electronics company. Since 1990, he has been an Associate Professor in the Department of Electronic Engineering, Technical University of Catalonia, Barcelona, Spain. His research interests include power-factor-correction circuits, active power filters, uninterruptible power systems, distributed power systems, and nonlinear control.

Prof. Matas was a recipient of ISI Highly Cited Researcher Award in 2014.



Y. A. Al-Turki received the Ph.D. degree in power systems from the University of Manchester, Manchester, U.K., in 1985.

Since 1999, he has been a Professor with the Department of Electrical and Computer Engineering, King Abdulaziz University, Jeddah, Saudi Arabia, where he is currently the Dean of Research. His current research interests include system modeling, power system dynamics, renewable energy, and microgrids.